

# NGC 6309, a planetary nebula that shifted from round to multipolar<sup>★†</sup>

G. Rubio,<sup>1</sup> R. Vázquez,<sup>2</sup> G. Ramos-Larios,<sup>3‡</sup> M. A. Guerrero,<sup>4</sup> L. Olgún,<sup>5</sup>  
P. F. Guillén<sup>2</sup> and H. Mata<sup>1</sup>

<sup>1</sup>CUCEI, Universidad de Guadalajara, Blvd Marcelino García Barragán 1421, 44430 Guadalajara, Jalisco, Mexico

<sup>2</sup>Instituto de Astronomía, Universidad Nacional Autónoma de México, Apdo. Postal 877, 22800 Ensenada, BC, Mexico

<sup>3</sup>Instituto de Astronomía y Meteorología, CUCEI, Universidad de Guadalajara, Av. Vallarta No. 2602, Col. Arcos Vallarta, 44130 Guadalajara, Jalisco, Mexico

<sup>4</sup>Instituto de Astrofísica de Andalucía, IAA-CSIC, C/Glorieta de la Astronomía s/n, E-18008 Granada, Spain

<sup>5</sup>Depto. de Investigación en Física, Universidad de Sonora, Blvd Rosales Esq. L. D. Colosio, Edif. 3H, 83190 Hermosillo, Sonora, Mexico

Accepted 2014 October 17. Received 2014 October 8; in original form 2014 August 29

## ABSTRACT

We present new narrow-band  $H\alpha$ ,  $[N\text{ II}]$ , and  $[O\text{ III}]$  high-resolution images of the quadrupolar planetary nebula NGC 6309 that show in great detail its bipolar lobes and reveal new morphological features. New high- and low-dispersion long-slit spectra have been obtained to help in the investigation of the new nebular components. The images and spectra unveil two diffuse blobs, one of them located  $\simeq 55$  arcsec from the central star along the NE direction ( $PA = +71^\circ$ ) and the other at  $\simeq 78$  arcsec in the SW direction ( $PA = -151^\circ$ ). Therefore, these structures do not share the symmetry axes of the inner bipolar outflows. Their radial velocities relative to the system are quite low:  $+3$  and  $-4$   $\text{km s}^{-1}$ , respectively. Spectroscopic data confirm a high  $[O\text{ III}]$  to  $H\beta$  ratio, indicating that the blobs are being excited by the UV flux from the central star. Our images convincingly show a spherical halo 60 arcsec in diameter encircling the quadrupolar nebula. The expansion velocity of this shell is low,  $\leq 6$   $\text{km s}^{-1}$ . To study the formation history of NGC 6309, we have used our new images and spectra, as well as available echelle spectra of the innermost regions, to estimate the kinematical age of each structural component: the software *SHAPE* has been used to construct a morphokinematic model for the ring and the bipolar flows that implies an age of  $\sim 4000$  yr, the expansion of the halo sets a lower limit for its age  $\geq 46\,000$  yr, and the very low expansion of the blobs suggests they are part of a large structure corresponding to a mass ejection that took place  $\sim 150\,000$  yr ago. In NGC 6309, we have direct evidence of a change in the geometry of mass-loss, from spherical in the halo to axially symmetric in the two pairs of bipolar lobes.

**Key words:** ISM: jets and outflows – ISM: kinematics and dynamics – planetary nebulae: individual: NGC 6309.

## 1 INTRODUCTION

Planetary nebulae (PNe) are the progeny of low- and intermediate-mass stars ( $0.8\text{--}1.0 M_\odot \leq M_i \leq 8\text{--}10 M_\odot$ ). The interacting stellar winds (ISW) model has been the canonical scenario to explain their formation and evolution (Kwok, Purton & Fitzgerald 1978). In the ISW model, the formation of bipolar or axisymmetric PNe requires

the presence of a density gradient between the equatorial and polar directions (Balick 1987). The discovery of highly elongated PNe (e.g. KJpn 8; López, Vázquez & Rodríguez 1995), high-velocity outflows (e.g. NGC 2392; Gieseking, Becker & Solf 1985), and PNe with multiple symmetry axes (e.g. the quadrupolar PNe, Manchado, Stanghellini & Guerrero 1996) has caused many problems for the ISW model (Balick & Frank 2002).

In this sense, there have been proposals of alternative or additional mechanisms that contribute to the formation and evolution of PNe, particularly for the ejection of precessing highly collimated outflows. These models include the interaction of a binary system (Soker & Livio 1994) that may give rise to accretion of material on to an equatorial disc, or the action of strong magnetic fields (García-Segura et al. 1999). Whatever the actual mechanism is, it is generally accepted that the onset of asymmetry occurs at the end of

<sup>★</sup>Based on observations made with the Nordic Optical Telescope, operated by the Nordic Optical Telescope Scientific Association at the Observatorio del Roque de los Muchachos, La Palma, Spain, of the Instituto de Astrofísica de Canarias.

<sup>†</sup>Based upon observations acquired at the Observatorio Astronómico Nacional in the Sierra San Pedro Mártir (OAN-SPM), Baja California, Mexico.

<sup>‡</sup>E-mail: [grubio@idec.edu.mx](mailto:grubio@idec.edu.mx)

**Table 1.** NOT ALFOSC optical observations of NGC 6309.

Filter	$\lambda_c$ (Å)	$\Delta\lambda$ (Å)	Exp. time (s)	Frames	Date
[O III]	5007	30	300	2	2009 July 21
H $\alpha$	6567	8	450	2	2009 July 21
[N II]	6588	9	450	2	2009 July 21
[O III]	5007	30	200	3	2014 July 18
[O III]	5007	30	450	3	2014 July 18

the asymptotic giant branch (AGB) or in the short transition from the AGB to the post-AGB phase. Collimated outflows seem to play a significant role in this process (Sahai & Trauger 1998).

Quadrupolar and multipolar PNe and those exhibiting collimated outflows at different directions are key, as precession can be linked to the final evolution of its progenitor star and its interaction with a binary companion or the occurrence of magnetic fields (Corradi et al. 2014; Tocknell, De Marco & Wardle 2014). One singular object is NGC 6309 (a.k.a. the Box Nebula), a recently recognized quadrupolar PN consisting of a central ring and two pairs of bipolar lobes aligned along different directions (Vázquez et al. 2008, hereafter V08). Interestingly, there were also hints for the presence of an outer structure around these bipolar lobes, defined as a halo by V08 in the basis of their narrow-band images. Additional evidence for this outer shell is found in the spectroscopic echelle observations of Chu & Jacoby (1989) who reported the presence of a slowly expanding outer shell.

In this paper, we revisit NGC 6309 to confirm the presence of the outer structures hinted by V08. Deep, high-resolution narrow-band images have allowed us to find a round halo that encircles the inner quadrupolar lobes. Much fainter nebular emission is found at large distances from the central star. Low- and high-dispersion optical spectra have been used to investigate the nature of these morphological components. The paper is organized as follows: Section 2 describes the new observations, the results are presented in Section 3, and the nature of the new features and the formation history of the nebula are discussed in Section 4. A final summary is presented in Section 5.

## 2 OBSERVATIONS

### 2.1 High-resolution imagery

New narrow-band optical images of NGC 6309 were obtained on 2009 July 21 using the Andalucía Faint Object Spectrograph and Camera (ALFOSC) at the 2.5-m Nordic Optical Telescope (NOT) of the Roque de los Muchachos Observatory (ORM, La Palma, Spain). The images were acquired through narrow-band filters that isolate the H $\alpha$  ( $\lambda_c = 6567\text{Å}$ , FWHM = 8 Å), [N II] ( $\lambda_c = 6588\text{Å}$ , FWHM = 9 Å), and [O III] ( $\lambda_c = 5007\text{Å}$ , FWHM = 30 Å) emission lines. The detector was a 2048 × 2048 EEV CCD with a pixel size of 13.5  $\mu\text{m}$ , which implies a plate scale of 0.184 arcsec pix<sup>-1</sup> and a field of view (FoV) of 6.6 arcmin × 6.6 arcmin. Exposure times were 900, 900, and 600 s for the H $\alpha$ , [N II], and [O III] images, respectively (Table 1). The images were processed using standard IRAF<sup>1</sup> routines. Composite colour-pictures of these images are shown

<sup>1</sup> IRAF is distributed by the National Optical Astronomy Observatory, which is operated by the Association of Universities for Research in Astronomy (AURA) under cooperative agreement with the National Science Foundation.

in Figs 1 and 2. The mean spatial resolution, as determined from the FWHM of stars in the FoV, was 0.7 arcsec.

A deep [O III] image was obtained on 2014 July 18 also using ALFOSC at the NOT. This time, the EEV CCD pixels were binned by three into pixels corresponding to a plate scale of 0.552 arcsec. Three 200 and three 450 s exposures were obtained for a total integration time of 1950 s (Table 1) in the search for faint outer structures. The image was similarly processed using standard IRAF routines and the spatial resolution implied by field stars was alike,  $\sim 0.8$  arcsec.

### 2.2 Long-slit low-dispersion spectroscopy

Low-resolution, long-slit spectra were obtained with the Boller & Chivens spectrograph mounted on the 2.1 m telescope at the Observatorio Astronómico Nacional in the Sierra San Pedro Mártir (OAN-SPM, Baja California, Mexico) on 2014 May 20 and 21. An E2V CCD (13.5  $\mu\text{m pix}^{-1}$ ) with 2048 × 2048 pixel array was used as detector. The 400 lines mm<sup>-1</sup> grating was used along with a 2.6 and 3.9 arcsec slit width, yielding a spectral resolution of 4.2 and 5.2 Å (FWHM), respectively. We have obtained three spectra on each position with an exposure time of 1800 s for each spectra, and combined them to get the median spectrum. The two slit position are indicated in Fig. 2 at PA = +155° and PA = +107°. The first slit covers the NE blob (hereafter blob A) and the second the SW blob (hereafter blob B). In both cases the brighter part of the emission region in [O III] $\lambda$ 5007 was included. The median spectrum was then subtracted from individual spectrum to detect and eliminate cosmic rays manually. Cleaned spectra were then added in order to get the final spectrum. Spectra reduction was carried out following standard procedures in XVISTA.<sup>2</sup>

### 2.3 Long-slit echelle spectroscopy

Two high-resolution long-slit spectra shown in Fig. 3, were obtained on 2013 May 19 with the Manchester Echelle Spectrograph (Meaburn et al. 2003) in the 2.1-m telescope at OAN-SPM. An E2V 13.5- $\mu\text{m pix}^{-1}$  CCD with 2048 × 2048 pixels was used as detector in 4 × 4 binning mode resulting in a spatial scale of 0.702 arcsec pix<sup>-1</sup> and a spectral scale of 0.087 Å pix<sup>-1</sup>. The spectra were centred at the [O III] $\lambda$ 5007 emission line using a filter ( $\Delta\lambda = 60\text{Å}$ ) to isolate the 114th order. Exposure time was 1800 s for each spectrum. The two slit position are indicated in Fig. 2 at PA = 64° (NE, solid line) and PA = +50° (SW, solid line).

Data were calibrated using IRAF standard procedures for long-slit spectroscopy. The slit width was 150  $\mu\text{m}$  (1.9 arcsec). The resulting spectral resolution (FWHM) is  $\simeq 12\text{ km s}^{-1}$  (accuracy  $\pm 1\text{ km s}^{-1}$ ), as measured from the lines of the ThAr calibration lamp. Seeing was  $\sim 2$  arcsec during the observations.

## 3 RESULTS

We have in hand kinematical and spatial information of the main structural components of NGC 6309: the bipolar lobes and central ring, the halo, and the outermost blobs. This information can be used to derive the kinematical ages of each component in order

<sup>2</sup> XVISTA was originally developed as Lick Observatory Vista. It is currently maintained by Jon Holtzman at New Mexico State University and is available at <http://ganymede.nmsu.edu/holtz/xvista>.

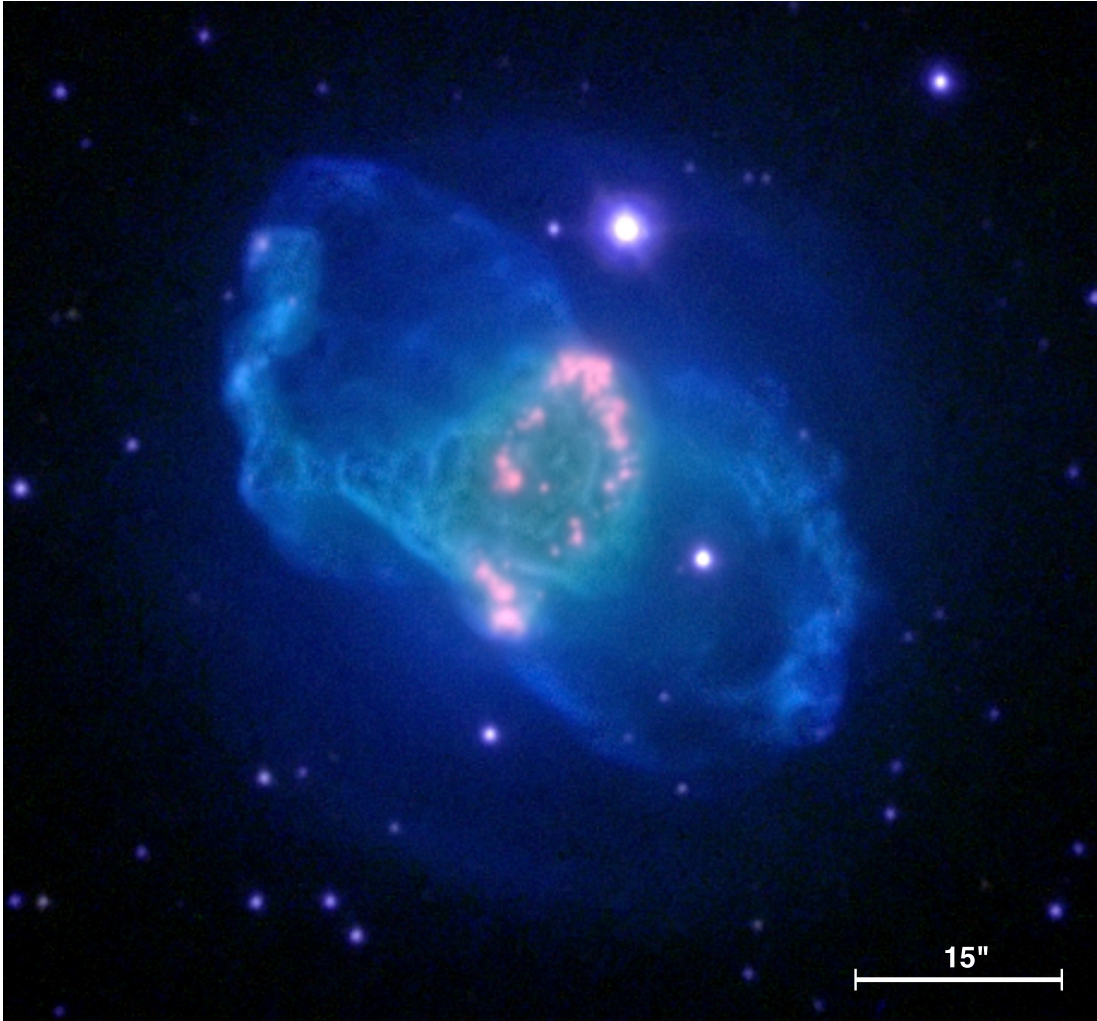


**Figure 1.** Colour-composite NOT picture of NGC 6309 in the [N II] (red), H $\alpha$  (green), and [O III] (blue) emission lines. This new picture reveals into great detail the fragmented emission of [N II] from the central ring, the bipolar lobes, and the outer round shell (the reddish colour of the central star is a processing artefact). North is up, east to the left.

to investigate their formation history. In the next subsections, we consider each component in turn.

### 3.1 The bipolar lobes: spatiokinematical modelling

The central regions of NGC 6309 were studied in detail by V08 using narrow-band images and high-dispersion echelle spectra. They concluded that the inner bright structure can be interpreted as an expanding torus and two pairs of bipolar lobes oriented along PAs 40° and 72°. These structures are revealed with unprecedented detail in the high-resolution images presented in Fig. 1. The central ring, which is the brightest structure, seems to be formed by a non-uniform assembly of knots especially prominent in [N II], that can be fairly fitted by an ellipse 20 arcsec  $\times$  8 arcsec in size. The conical eastern structure reported by V08 after the use of ‘unsharp-masking’ techniques is plainly evident in our direct images. It connects the ring-like central structure to the north-east arm described in old, low resolution imagery. A possible western counterpart is absent. The bipolar lobes are composed by small gaseous ‘flakes’ and their tips display a characteristic wave-like pattern. The two pairs of bipolar lobes, which were discovered by their distinct kinematics using

long-slit echelle data (V08), are neither obvious features, but they can be hinted in this direct image.

Using the simple hourglass model of Solf & Ulrich (1985), and assuming a distance of 2 kpc, V08 derived kinematical ages  $\sim$ 4000 and  $\sim$ 3700 yr for the bipolar lobes along PA 40° and 72°, respectively. The inclination angle with respect to the line of sight was estimated to be 66° from the assumption that the axis of symmetry of the lobe at PA 72° coincides with the main axis of the ring, for a deprojected expansion velocity of the ring of 25 km s $^{-1}$ . Using the software SHAPE (Steffen et al. 2011), specifically designed for the spatiokinematical modelling of expanding nebulae, we have fit our images and the high-dispersion spectra presented by V08 adopting a sophisticated model that includes two irregular bipolar lobes and an expanding ring. The deviations of the bipolar lobes from Solf & Ulrich’s (1985) prescription are modelled using the BUMP modifier in the SHAPE software. The synthetic image implied by the best-fitting model is presented in Fig. 4.

The best-fitting model parameters listed in Table 2 represent small adjustments with respect to those presented by V08. In particular, the estimate of the kinematical ages of the bipolar lobes remains unchanged.



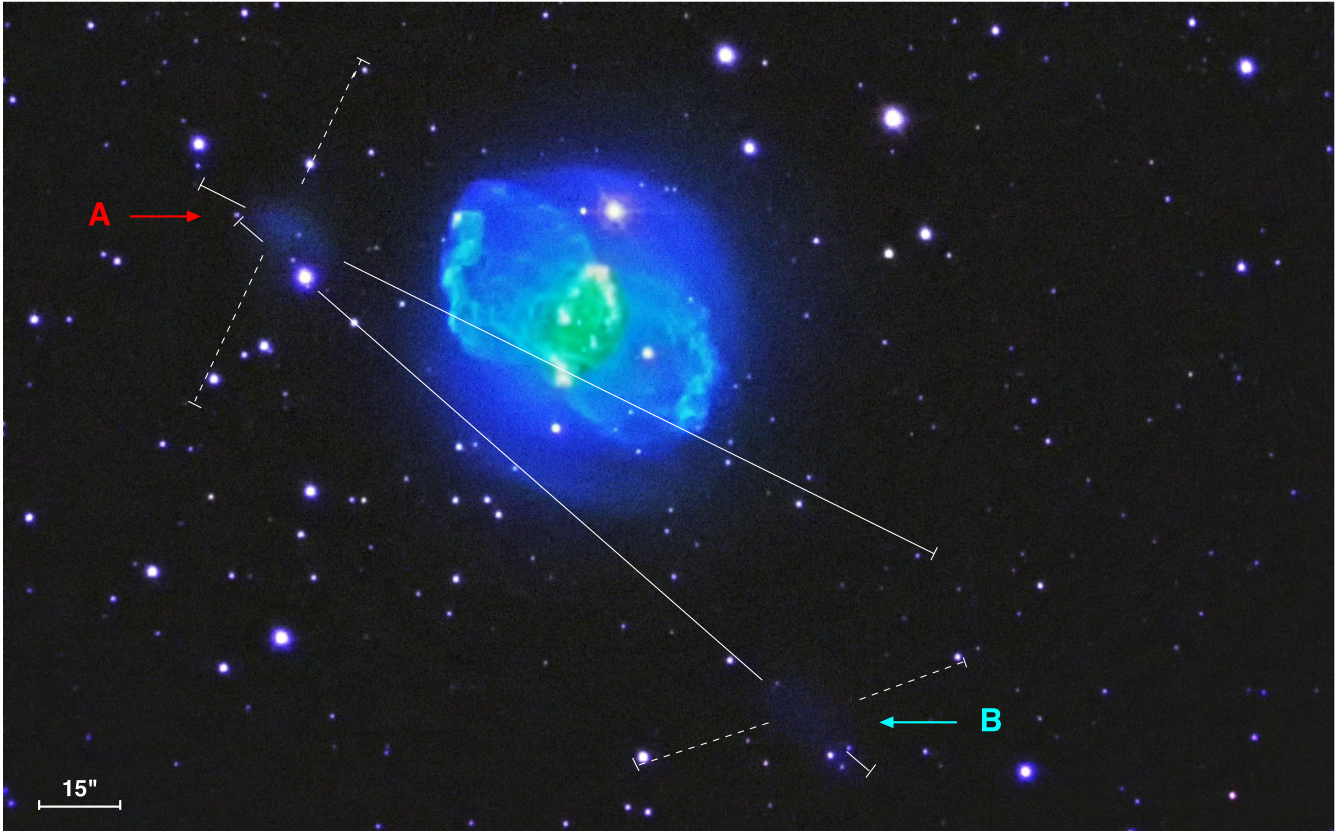


**Figure 2.** Same as Fig. 1, but for a larger FoV. The outer blobs ‘A’ and ‘B’ are labelled. The dotted lines mark the position of the slits used for low-dispersion spectroscopy, whereas the solid lines mark that of the high-dispersion spectra, corresponding at 160 arcsec length.

**Table 2.** Parameters of main structures measured and derived from models. All values correspond to deprojected parameters.

Parameter	Ring PA 72°	Bipolar outflow PA 40°	Bipolar outflow PA 72°
Semimajor axis (arcsec)	10	35	28
Equatorial velocity (km s <sup>-1</sup> )	25	25	25
Polar velocity (km s <sup>-1</sup> )	–	84	72
Main axis inclination (°)	66	66	66
Kinematical age (yr)	3800	3950	3750

### 3.2 The faint halo

The new narrow-band images of NGC 6309 shown in Figs 1 and 2 clearly unveil a shell surrounding the bipolar lobes. This shell, which we will recall as the halo of NGC 6309 following V08, has a round appearance, with a size  $\sim 60$  arcsec. The shell is only detected in the [O III] image, while remaining unseen in the H $\alpha$  and [N II] images. The shell shows a distinctive limb-brightened arc towards the North-west, whereas it fades progressively along all other directions. This is illustrated in Fig. 5, which shows the halo’s surface brightness profile extracted along the north-west–south-east direction. The halo surface brightness is  $\sim 100$  times fainter than the central region of the nebula.

The presence of this structural component of NGC 6309 was previously reported by V08, that described it as a diffuse halo, but could not provide too much detail. Actually, it was Chu & Jacoby (1989) the first who reported the presence of an extended shell around the bright innermost regions of NGC 6309 based on echelle

data. They computed an expansion velocity  $\sim 5$  km s<sup>-1</sup> using the line width from their long-slit echelle spectrum.

It is interesting to revisit this expansion velocity to gain a better understanding of the evolutionary past of NGC 6309. The faint halo around the bright bipolar lobes is registered by the long-slit echelle spectrum covering blob B (Fig. 3 upper-right panel). This spectrum shows an unresolved [O III] line. We have computed the line width in space bins of 5 pixels ( $\sim 3.5$  arcsec) and found that the FWHM is rather constant,  $21.0 \pm 1.5$  km s<sup>-1</sup>. After subtract the instrumental and thermal width, as described by Bryce et al. (1992), it results in an FWHM of  $17.2 \pm 1.5$  km s<sup>-1</sup>. The variance of the line width can be used to derive an upper limit for the expansion velocity (Guerrero, Villaver & Manchado 1998) as the line width can be expected to increase with the path length of the shell along the line of sight. The shell appearance and its surface brightness imply it is a filled shell. Assuming constant emissivity, we have estimated an upper limit for the expansion velocity along the line of sight of  $5.75$  km s<sup>-1</sup>. After correcting for projection effects, and assuming a distance of 2 kpc this implies an upper limit to the expansion velocity of  $< 6.1$  km s<sup>-1</sup> and a lower limit to the expansion age, for a shell radius of 30 arcsec, of  $> 46$  000 yr, comparable to the [O III] halo expansion velocity of NGC 6543 (Bryce et al. 1992).

A relevant aspect is that the halo’s centre, as determined by an [O III] brightness contour at low intensity, does not line up with the central star. This offset suggests that the star presents a proper motion along the north-east direction. Moreover, the bipolar structure protrudes into the NE edge of the halo, which provides another element to support this hypothesis. The estimation of the direction

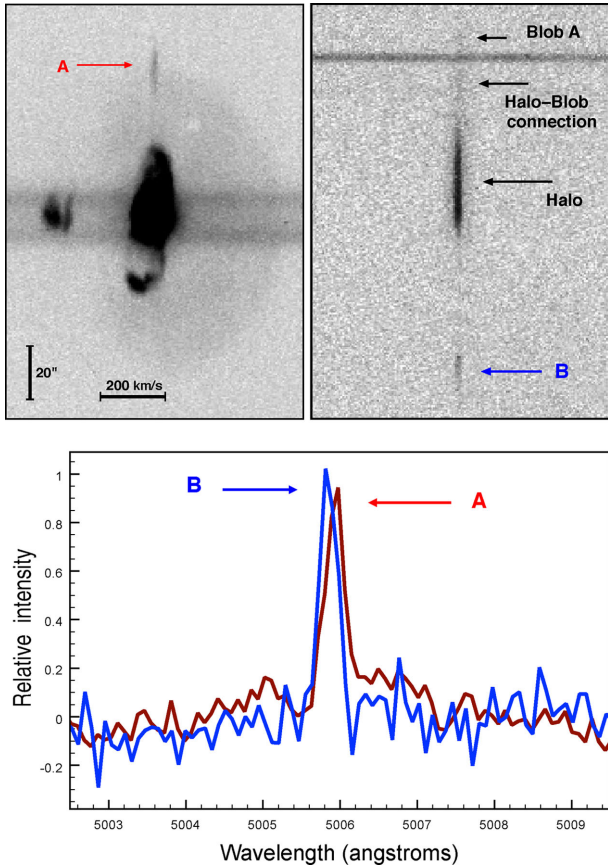


**Figure 3.** Top: echellograms of slits at PA  $+64^\circ$  across blob A (left) and PA  $+50^\circ$  across blob B and halo (right). The blob A is barely visible in the right image because the slit passes slightly below the blob (see Fig. 2). The spatial location of the blobs, halo, and halo–blob connection are labelled. Bottom: one-dimensional averaged spectra of blobs A and B corresponding at 28 arcsec and centred at the peak emission were extracted from the echellograms in top panels.

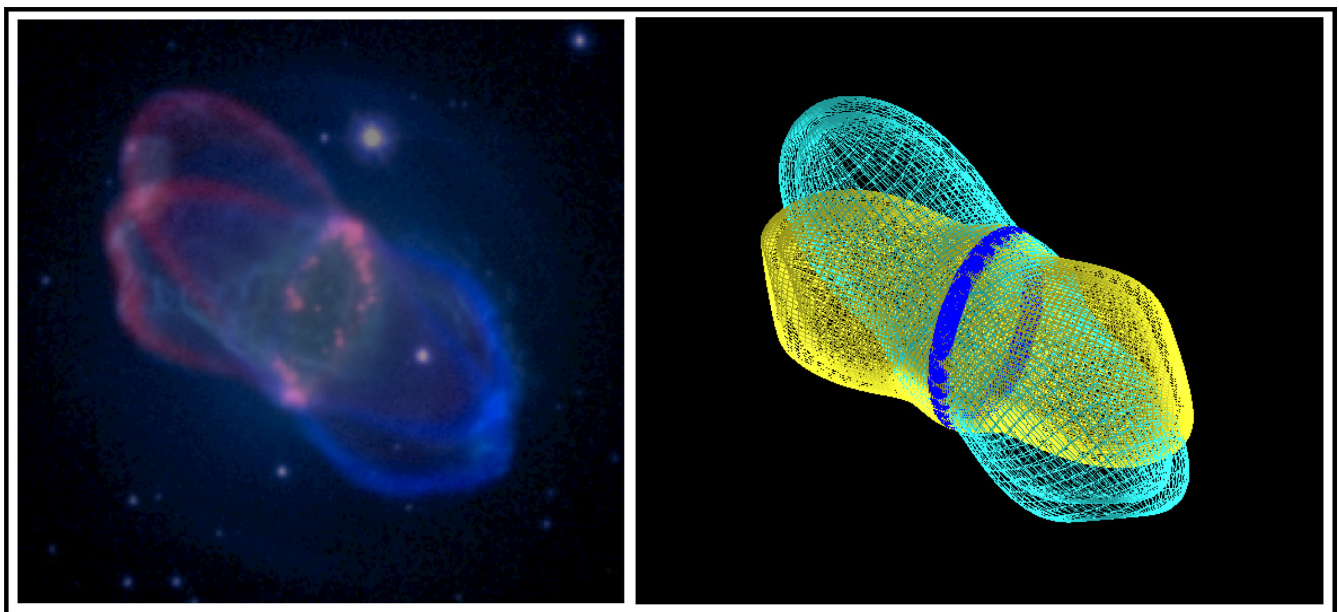


**Figure 4.** Structure model of NGC 6309 produced with SHAPE. Left: model superimposed on the composite RGB image. Right: the model formed by two bipolar outflows and an expanding ring.

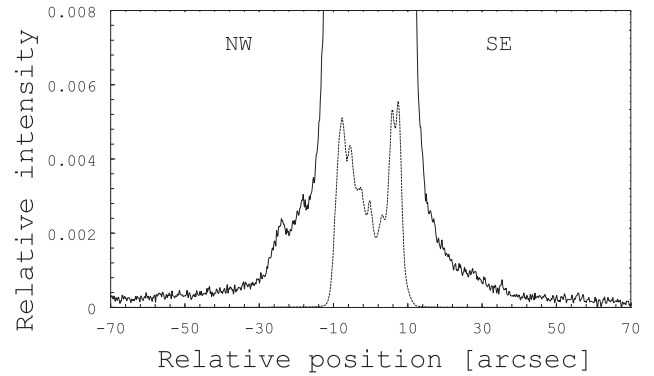


**Figure 5.** [O III] surface brightness profile of the halo of NGC 6309 along the north-west–south-east direction at PA  $= -30^\circ$ . The profile has been extracted using an aperture of width 1.8 arcsec in order to attain an adequate signal-to-noise ratio. The halo’s profile is normalized to the emission peak.

of the movement of the star from the relative position of the halo centre differs from the north-west direction reported by Kerber et al. (2008), also, the external halo show a kind of bright non-diffuse rim in the NW direction (see Fig. 2). We attribute this inconsistency to the difficulties to determine the position of the central star in a region with bright and irregular diffuse emission.

### 3.3 The blobs

The large FoV image of NGC 6309 presented in Fig. 2 reveals two faint blobs: the eastern blob ‘A’ is located at 55 arcsec from the Central Star of Planetary Nebula (CSPN) along PA  $\approx 70^\circ$ , whereas the western blob ‘B’ is located at 78 arcsec along PA  $\approx 210^\circ$ . Therefore, they are not located symmetrically with respect to the nebular centre. They have a size of 20 arcsec  $\times$  10 arcsec and their appearance is diffuse, without any distinctive feature.

The blobs emit predominantly in [O III], with blob A being brighter than blob B. The averaged surface brightness is



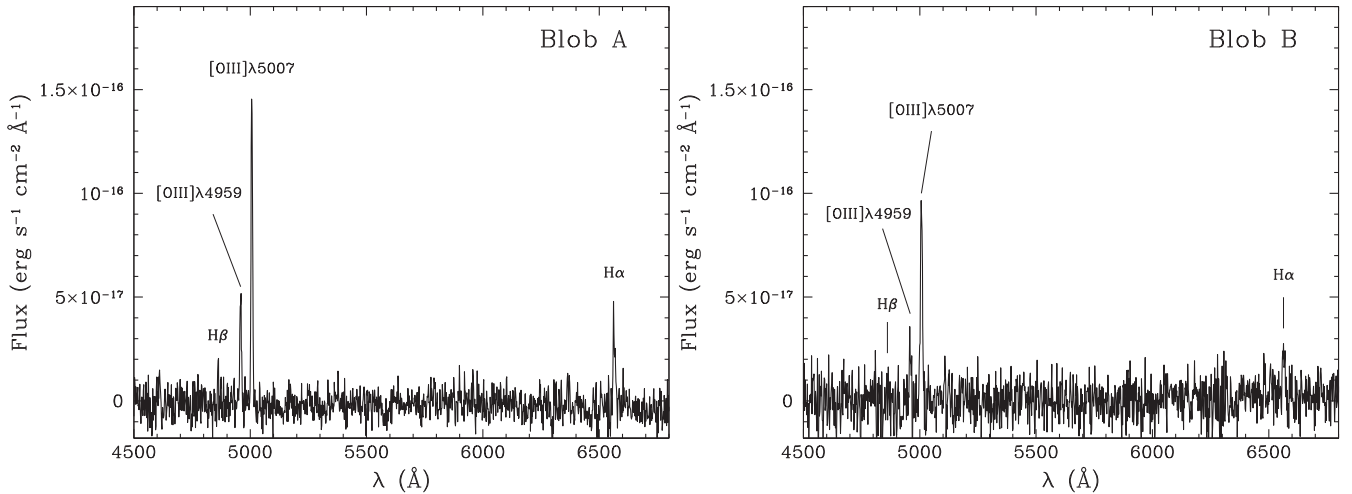


**Figure 6.** One-dimensional spectra extracted from the blobs A and B. Aperture regions of  $2.6 \text{ arcsec} \times 14.2 \text{ arcsec}$  and  $3.9 \text{ arcsec} \times 17.7 \text{ arcsec}$  centred on blob A and B have been used, respectively.

$1.8 \times 10^{-13} \text{ erg cm}^{-2} \text{ s}^{-1} \text{ arcsec}^{-2}$  for blob A and  $8.3 \times 10^{-14} \text{ erg cm}^{-2} \text{ s}^{-1} \text{ arcsec}^{-2}$  for blob B. Spectra of both blobs are shown in Fig. 6. The  $[\text{O III}] \lambda\lambda 4959, 5007$  emission lines can clearly be seen in both blobs. In the brightest blob A, faint  $\text{H}\alpha$  and  $\text{H}\beta$  emission was also detected, while in blob B  $\text{H}\alpha$  was detected, but  $\text{H}\beta$  appears marginal. In general blob B shows fainter emission at all the lines.

The low-dispersion spectra (Fig. 6) imply  $[\text{O III}]$  to  $\text{H}\beta$  ratios similar to those reported by V08 for the central regions. This seems to suggest that the blobs are excited by the UV flux of the central star. On the other hand, the  $\text{H}\alpha$  to  $\text{H}\beta$  ratio is smaller than in the central nebula, indicating lower extinction. Indeed, a logarithmic extinction coefficient  $c_{\text{H}\beta}$  of 0.25 is derived for blob A, whereas for the central region of NGC 6309 it is estimated to be 0.90 (Vázquez et al. 2008).

The echelle spectra provide valuable information on the kinematics of these blobs. The one-dimensional averaged spectra extracted for each blob reveal a small although significant difference in their radial velocities (Fig. 3). The peak emission of blob A is redshifted, with a systemic velocity<sup>3</sup>  $V_A = +3 \text{ km s}^{-1}$ , whereas the emission peak of blob B is blueshifted,  $V_B = -4 \text{ km s}^{-1}$ . The two-dimensional echellograms show the blobs to be almost inert, with internal velocity variations within the line-width, i.e. without significant kinematical structure.

A close inspection of the echellogram along blob B (Fig. 3, top-right) reveals weak emission connecting blob A to the halo of NGC 6309. This connection is clearly shown in the intensity profile of the  $[\text{O III}]$  extracted from this echelle spectrum (Fig. 7). Blob A is thus not isolated, but it is connected to the halo of NGC 6309. This physical connection and the similarity between the radial velocity of the blobs and that of NGC 6309, and their excitation degree strongly support the association of the blobs with NGC 6309.

A deep  $[\text{O III}]$  image (second observation, see Section 2.1) reveals weak flocculent structures in the southern part of the halo. These features, not shown here, are not completely undisputed, as we recognize they may be caused by light dispersed from the

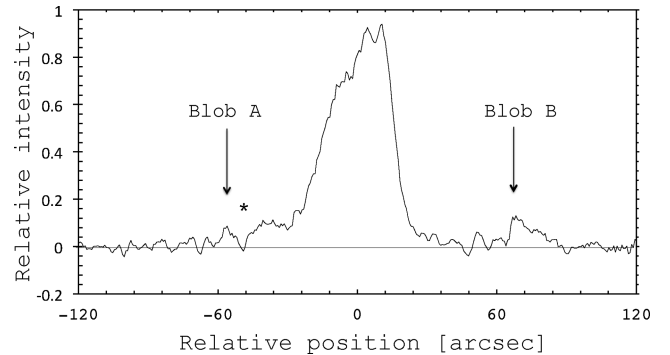


**Figure 7.** Intensity profile extracted from the echellogram corresponding to the slit at  $\text{PA} = +50^\circ$  (Fig. 3, upper-right panel). The link between the halo and blob A is clearly seen. The position of an overextracted star is shown.

bright inner nebular by different optical elements of the telescope and camera (see Corradi et al. 2003, for a thorough discussion on the difficulties of detecting faint nebular features around bright PNe).

## 4 DISCUSSION

The quality of the narrow-band images of NGC 6309 presented in this work has allowed us to obtain a precise description of morphological features that were only hinted in previous studies (the eastern conical structure, the round halo) or simply undetected (the outer faint blobs). The spectroscopic information gathered here can be used to shed light into the origin of these structures and to investigate the formation history of this PN.

### 4.1 The origin of the faint outer blobs

The nature of the faint outer blobs A and B is really intriguing. The spatial, spectroscopic, and kinematical information provided in Section 3.2 can be put to the test different scenarios to assess their origin.

It is certainly appealing to identify blobs A and B with high-velocity polar ejections. High-velocity knots located at several or

<sup>3</sup> The radial velocity is referred to the systemic velocity, as derived by V08,  $V_{\text{LSR}} = -32 \pm 2 \text{ km s}^{-1}$ .

many radii of the main nebular shell have been identified in a number of PNe, e.g. Fleming 1 and MyCn 18 (López, Meaburn & Palmer 1993; Bryce et al. 1997). In some cases, there is evidence of the interaction of these outflows with the nebular shell (e.g. NGC 6778; Guerrero & Miranda 2012). Blobs A and B may have interacted with the bipolar lobes of NGC 6309: blob A is aligned with the eastern conical structure and the CSPN, whereas blob B and the CSPN are aligned with an opening in the southwestern region of the bipolar lobe. This would imply that the blobs, having played a role in the formation of the bipolar lobes (Sahai & Trauger 1998), are coeval to those or followed immediately their formation. Since the bipolar lobes have expansion velocities  $\sim 80 \text{ km s}^{-1}$  and angular extents two to three times smaller than the radial distances of blobs A and B to the CSPN, we can infer expansion velocities of these blobs in excess of  $160\text{--}240 \text{ km s}^{-1}$ . As their systemic velocity is only  $3\text{--}4 \text{ km s}^{-1}$ , the inclination angle with respect to the plane of the sky must be  $\approx 1^\circ$ . This seems very unlikely, especially because blobs A and B are oriented along different directions. Furthermore, the diffuse appearance of the blobs is in sharp contrast with the bow-shock (e.g. IC 4694; Guerrero et al. 2008) or compact, knotty morphologies (e.g. KjPn 8; López et al. 1997) exhibited by fast outflows of PNe. We therefore disregard the idea that blobs A and B are fast collimated outflows.

Alternatively, blobs A and B can be interpreted as material of the ISM which is illuminated and ionized by the CSPN of NGC 6309. Their excitation degree is high, with [O III] to H $\beta$  ratios similar to those of the inner nebula, thus supporting this hypothesis. If so, the alignment of these blobs with particular nebular features suggests that they correspond to openings in the nebular shell that allow a greater UV flux to escape. The lower extinction of blobs A and B, as compared to that of NGC 6309, suggests that the main nebular shell suffers from internal obscuration.

It is interesting to note that the radial velocity of these blobs and that of NGC 6309 main nebular shell are very similar. Whereas this does not rule out the possibility that blobs A and B belong to the ISM, it hints at a real physical connection between the blobs and the PN. This link is strengthened by the emission connecting blob A with the halo of NGC 6309. The two blobs can be part of a large and faint structure around NGC 6309 ejected at low speeds in the early evolution of the PN (Olofsson et al. 2000). Assuming a distance of 2 kpc, and an expansion velocity of  $5 \text{ km s}^{-1}$ , consistent with their radial velocity, a kinematical age of 150 000 yr can be derived. This would place this ejection in the late thermal pulse phase of the AGB (Vassiliadis & Wood 1993; Stanghellini & Pasquali 1995). The blobs would be the brightest regions of this structure or sections that are illuminated preferentially by the CSPN through holes in the nebular shell. Examples of incomplete haloes (e.g. IC 4593; Corradi et al. 1997) or inhomogeneous haloes (e.g. NGC 6543; Middlemass, Clegg & Walsh 1989) abound in the literature.

#### 4.2 NGC 6309: a case study of the change in mass-loss geometry in a PN

The formation history of NGC 6309 is certainly exceptional. Some 150 000 yr ago, its central star seemed to undergo a mass-loss event which resulted in a large, slowly expanding shell-like structure. Only the brightest regions of this structure or those regions that are preferentially illuminated by the CSPN have been detected so far as blobs A and B. The long time-scale and slow expansion velocity can be used to identify this ejection with one of the last thermal pulses experienced by the progenitor star in the late AGB phase.

More recently,  $\sim 45\,000$  yr ago, the star experienced another episode of heavy mass-loss that resulted in the formation of its halo. This mass ejection had a clear spherical symmetry which is only distorted by the possible interaction of the nebula with the ISM, producing the arc-like feature along the direction of the motion of the CSPN. The halo may correspond to the very last thermal pulse in the late AGB phase.

The transformation of the AGB star into a PN occurred  $\sim 4000$  yr ago. The star suffered a heavy mass-loss episode that ejected its envelope and produced the bipolar lobes. At some moment between the ejection of the nebular halo and that of the bright inner nebula, the geometry of the mass-loss experienced a dramatic change, from spherically symmetric to axially symmetric, with rapid changes in the symmetry axis that produced two pairs of bipolar lobes along different directions. The change in mass-loss geometry experienced by the progenitor of NGC 6309 is consistent with the mechanism proposed by Sahai & Trauger (1998) to explain the onset of asymmetry: fast ( $\sim 100 \text{ km s}^{-1}$ ) collimated outflows ejected in the late AGB phase carve through the AGB envelope to produce polar or multipolar impressions in the previously spherical envelope. The onset of the fast stellar wind will bore through these openings in the nebular envelope to shape axially symmetric PNe.

This scenario is in agreement with the presence of round haloes detected in bipolar proto-PNe such as IRAS 13557–6442, IRAS 17253–2831, IRAS 17440–3310, IRAS 19306+1407 (Sahai et al. 2007a), and in the quadrupolar proto-PN IRAS 19475+3119 (Sahai et al. 2007b). Whereas the inner bipolar nebula and outer halo configuration seems common in early stages of PN formation (Su 2004), there is little evidence in evolved bipolar PNe. Besides the H $_2$  halo detected around NGC 2440 (Ramos-Larios & Phillips 2009), there are no other bipolar PN surrounded by a round halo (e.g. Chu, Jacoby & Arendt 1987; Corradi & Schwarz 1993). Round rings and arcs have been detected around the central regions of Hb 5, NGC 6881, and NGC 7026 (Corradi et al. 2004), but their sizes are smaller than the bipolar nebulae and they tend to have significantly weaker surface brightness than that of the nebular region. In this sense, the presence of a distinct spherical halo around a quadrupolar PN makes of NGC 6309 a rare case in the bestiary of axially symmetric PNe.

## 5 CONCLUDING REMARKS

We have presented new observations of NGC 6309 with deep, high-resolution images that reveal its internal structure in great detail, besides confirming the presence of a spherical halo. Likewise, we show unprecedented structures outside the main nebula, which we have termed blobs. We have carried out high- and low-dispersion spectroscopy to better understand the nature and kinematics of these morphological features.

NGC 6309 has a remarkable morphology and allows us to clearly see the record of different mass-loss episodes; the kinematics of the blobs reveals that these components probe an early mass ejection which took place during the thermal pulse phase,  $\approx 150\,000$  yr ago. The surrounding halo, seen clearly for the first time in our images, is the remnant of symmetrical mass-loss in the final stages of the AGB phase. The picture is completed with two pairs of bipolar lobes created during a short period 4000 yr ago. We emphasize the change in mass-loss geometry from the final stages of the AGB, when the round halo was ejected, to the early PN phase, when multiple bipolar lobes were ejected along different directions.

In order to investigate the origin of the late changes in mass-loss in NGC 6309, an exhaustive study of its CSPN is required to search

for variability or chemical abundances anomalies associated with its evolution through a common envelope phase. A study of dust polarization emission can also shed light in the search for magnetic fields. The study of the late evolution and formation of bipolar PNe will also benefit from the understanding of the low occurrence of round outer structures among these sources.

## ACKNOWLEDGEMENTS

We are grateful to the staff of OAN-SPM, specially to Gustavo Melgoza-Kennedy, telescope operator, for his assistantship during observations. This paper has been supported by grant PAPIIT-DGAPA-UNAM IN107914. GR acknowledges CONACYT for his graduate scholarship and the IAA for its hospitality during his stay. GR-L acknowledges support from CONACYT (grant 177864), CGCI, PROMEP and SEP (Mexico). MAG also acknowledges support from grant AYA 2011-29754-C03-02.

## REFERENCES

- Balick B., 1987, *AJ*, 94, 671  
 Balick B., Frank A., 2002, *ARA&A*, 40, 439  
 Bryce M., Meaburn J., Walsh J. R., Clegg R. E. S., 1992, *MNRAS*, 254, 477  
 Bryce M., Lopez J. A., Holloway A. J., Meaburn J., 1997, *ApJ*, 487, L161  
 Chu Y.-H., Jacoby G. H., 1989, in Torres-Peimbert S., ed., *Proc. IAU Symp.* 131, *Planetary Nebulae*. Dordrecht, Kluwer, p. 198  
 Chu Y.-H., Jacoby G. H., Arendt R., 1987, *ApJSS*, 64, 529  
 Corradi R. L. M., Schwarz H. E., 1993, *A&A*, 278, 247  
 Corradi R. L. M., Guerrero M., Manchado A., Mampaso A., 1997, *New Astron.*, 2, 461  
 Corradi R. L. M., Schönberner D., Steffen M., Perinotto M., 2003, *MNRAS*, 340, 417  
 Corradi R. L. M., Sánchez-Blázquez P., Mellema G., Giammanco C., Schwarz H. E., 2004, *A&A*, 417, 637  
 Corradi R. L. M. et al., 2014, *MNRAS*, 441, 2799  
 García-Segura G., Langer N., Różyczka M., Franco J., 1999, *ApJ*, 517, 767  
 Gieseking F., Becker I., Solf J., 1985, *ApJ*, 295, L17  
 Guerrero M. A., Miranda L. F., 2012, *A&A*, 539, A47  
 Guerrero M. A., Villaver E., Manchado A., 1998, *ApJ*, 507, 889  
 Guerrero M. A. et al., 2008, *ApJ*, 683, 272  
 Kerber F., Mignani R. P., Smart R. L., Wicenc A., 2008, *A&A*, 479, 155  
 Kwok S., 2000, *Cambridge Astrophysics Series: 33, The Origin and Evolution of Planetary Nebulae*. Cambridge Univ. Press, Cambridge  
 Kwok S., Purton C. R., FitzGerald P. M., 1978, *ApJ*, 219, L125  
 López J. A., Meaburn J., Palmer J. W., 1993, *ApJ*, 415, L135  
 López J. A., Vázquez R., Rodríguez L. F., 1995, *ApJ*, 455, L63  
 López J. A., Meaburn J., Bryce M., Rodríguez L. F., 1997, *ApJ*, 475, 705  
 Manchado A., Stanghellini L., Guerrero M. A., 1996, *ApJ*, 466, 95  
 Meaburn J., López J. A., Gutiérrez L., Quirós F., Murillo J. M., Valdez J., Pedrayes M., 2003, *Rev. Mex. Astron. Astrofis.*, 39, 185  
 Middlemass D., Clegg R. E. S., Walsh J. R., 1989, *MNRAS*, 239, 1  
 Olofsson H., Bergman P., Lucas R., Eriksson K., Gustafsson B., Bieging J. H., 2000, *A&A*, 353, 583  
 Peimbert M., 1978, in Terzian Y., ed., *Proc. IAU Symp.* 76, *Planetary Nebulae*. Kluwer, Dordrecht, p. 215  
 Ramos-Larios G., Phillips J. P., 2009, *MNRAS*, 400, 575  
 Sahai R., Trauger J. T., 1998, *AJ*, 116, 1357  
 Sahai R., Morris M., Sánchez Contreras C., Claussen M., 2007a, *AJ*, 134, 2200  
 Sahai R., Sánchez Contreras C., Morris M., Claussen M., 2007b, *ApJ*, 658, 410  
 Soker N., Livio M., 1994, *ApJ*, 421, 219  
 Solf J., Ulrich H., 1985, *A&A*, 148, 274  
 Stanghellini L., Pasquali A., 1995, *ApJ*, 452, 286  
 Steffen W., Koning N., Wenger S., Morisset C., Magnor M., 2011, *IEEE Trans. Vis. Comput. Graphics*, 17, 454  
 Su K. Y. L., 2004, in Meixner M., Kastner J. H., Balick B., Soker N., eds, *ASP Conf. Ser. Vol. 313, Asymmetrical Planetary Nebulae III: Winds, Structure and the Thunderbird*. Astron. Soc. Pac., San Francisco, p. 247  
 Tocknell J., De Marco O., Wardle M., 2014, *MNRAS*, 439, 2014  
 Vassiliadis E., Wood P. R., 1993, *ApJ*, 413, 641  
 Vázquez R., Miranda L. F., Olgún L., Ayala S., Torrelles J. M., Contreras M. E., Guillén P. F., 2008, *A&A*, 481, 107 (V08)

This paper has been typeset from a  $\text{\TeX}/\text{\LaTeX}$  file prepared by the author.